Compact bending sensor based on a fiber Bragg grating in an abrupt biconical taper

Wei Cui, Jinhai Si,* Tao Chen, and Xun Hou

Key Laboratory for Physical Electronics and Devices of the Ministry of Education & Shaanxi Key Lab of Information Photonic Technique, School of Electronics & information Engineering, Xi'an Jiaotong University, No.28, Xianning West Road, Xi'an, 710049, China.

jinhaisi@mail.xjtu.edu.cn

Abstract: We propose and experimentally demonstrate a compact bending sensor. The head of the sensor is only 0.8 mm in length, and consists of an abrupt biconical fiber taper formed using a conventional fusion splicer, in which a fiber Bragg grating (FBG) is inscribed using a femtosecond laser. The biconical taper incorporating the FBG can couple light from the cladding to the backward-propagating core mode, which realizes an interferometer in reflection-mode. Bending of the structure can be detected from the contrast change of interference fringes. A configuration to measure curvature is investigated to demonstrate the sensing characteristics. The temperature cross-sensitivity of the sensor is studied, and the results demonstrate that it is insensitive to temperature.

OCIS codes: (060.2370) Fiber optics sensors; (060.3735) Fiber Bragg gratings.

References and links

1. B. Lee, "Review of the present status of optical fiber sensors," Opt. Fiber Technol. **9**(2), 57–79 (2003).
2. Y. Rao, "In-fibre Bragg grating sensors," Meas. Sci. Technol. **8**(4), 355–375 (1997).
3. T. Guo, A. Ivanov, C. Chen, and J. Albert, "Temperature-independent tilted fiber grating vibration sensor based on cladding-core recoupling," Opt. Lett. **33**(9), 1004–1006 (2008).
4. T. Guo, L. Shao, H. Y. Tam, P. A. Krug, and J. Albert, "Tilted fiber grating accelerometer incorporating an abrupt biconical taper for cladding to core recoupling," Opt. Express **17**(23), 20651–20660 (2009).
5. Z. Yong, C. Zhan, J. Lee, S. Yin, and P. Ruffin, "Multiple parameter vector bending and high-temperature sensors based on asymmetric multimode fiber Bragg gratings inscribed by an infrared femtosecond laser," Opt. Lett. **31**(12), 1794–1796 (2006).
6. S. W. James and R. P. Tatam, "Optical fibre long-period grating sensors: characteristics and application," Meas. Sci. Technol. **14**(5), R49–R61 (2003).
7. S. Baek, Y. Jeong, and B. Lee, "Characteristics of short-period blazed fiber Bragg gratings for use as macro-bending sensors," Appl. Opt. **41**(4), 631–636 (2002).
8. W. Shin, Y. L. Lee, B. Yu, Y. Noh, and T. J. Ahn, "Highly sensitive strain and bending sensor based on in-line fiber Mach–Zehnder interferometer in solid core large mode area photonic crystal fiber," Opt. Commun. **283**(10), 2097–2101 (2010).
9. A. Cusano, M. Consales, A. Crescitelli, and A. Ricciardi, *Lab-On-Fiber Technology* (Springer, 2015).
10. L. Shao, A. Laronche, M. Smietana, P. Mikulic, W. J. Bock, and J. Albert, "Highly sensitive bend sensor with hybrid long-period and tilted fiber Bragg grating," Opt. Commun. **283**(13), 2690–2694 (2010).
11. Y. X. Jin, C. C. Chan, X. Y. Dong, and Y. F. Zhang, "Temperature-independent bending sensor with tilted fiber Bragg grating interacting with multimode fiber," Opt. Commun. **282**(19), 3905–3907 (2009).
12. T. Q. Jia, H. X. Chen, M. Huang, F. L. Zhao, J. R. Qiu, R. X. Li, Z. Z. Xu, X. K. He, J. Zhang, and H. Kuroda, "Formation of nanogratings on the surface of a ZnSe crystal irradiated by femtosecond laser pulses," Phys. Rev. B **72**(12), 125429 (2005).
13. D. Tan, S. Zhou, J. Qiu, and N. Khusro, "Preparation of functional nanomaterials with femtosecond laser ablation in solution," J. Photochem. Photobiol, C. Photo. **17**, 50–68 (2013).
14. R. R. Gattass and E. Mazur, "Femtosecond laser micromachining in transparent materials," Nat. Photonics **2**(4), 219–225 (2008).
15. J. Qiu, "Femtosecond laser-induced microstructures in glasses and applications in micro-optics," Chem. Rec. **4**(1), 50–58 (2004).
16. Z. Tian, S. S. Yam, and H. P. Loock, "Refractive index sensor based on an abrupt taper Michelson interferometer in a single-mode fiber," Opt. Lett. **33**(10), 1105–1107 (2008).
17. P. Lu, L. Men, K. Sooley, and Q. Chen, "Tapered fiber Mach–Zehnder interferometer for simultaneous measurement of refractive index and temperature," Appl. Phys. Lett. **94**(13), 131110 (2009).

#234537 - $15.00 USD Received 13 Feb 2015; revised 5 Apr 2015; accepted 6 Apr 2015; published 20 Apr 2015

18. J. D. Love, W. M. Henry, W. J. Stewart, R. J. Black, S. Lacroix, and F. Gonthier, "Tapered single-mode fibres and devices. Part 1: Adiabaticity criteria," IEE Proc. J Optoelectron. **138**(5), 343–354 (1991).
19. R. J. Black, S. Lacroix, F. Gonthier, and J. D. Love, "Tapered single-mode fibres and devices. part 2: experimental and theoretical quantification," IEE Proc. J Optoelectron. **138**(5), 355–364 (1991).

1. Introduction

Over the past decade, optical fibers have seen significant development, and have been employed in numerous and varied applications [1,2]. Fiber sensors are high-precision, low-cost, and are not affected by electromagnetic noise, making them strong competitors to conventional electronic sensors in many applications. Fiber bending sensors have attracted much attention, because of their applications in structural monitoring, accelerometers and displacement measurement [3,4]. To date, fiber bending sensors have been developed using a variety of structures, including asymmetric FBGs, long period gratings (LPGs), tilted fiber Bragg gratings (TFBGs), and Mach-Zehnder interferometers [5–8]. TFBG are advantageous because of the high sensitivity and low cross-sensitivity to other parameters. Baek et al. proposed a bending sensor based on a single TFBG, which utilizes change in the transmission loss of the cladding modes [7].

Reflection-mode fiber sensors are preferred in practical applications, because they require only one port, which provides greater flexibility and is less invasive in terms of installation [9].To make use of the cladding modes in reflection-mode with single-end access, some hybrid sensors combine a TFBG with a section of multimode fiber, or use an abrupt biconical taper or LPG in series [4,10,11]. Additional structures re-couple the cladding modes into the guided backward core mode to realize measurement in reflection-mode. The LPG and TFBG that have been employed in the sensors are relatively long (typically >10 mm). When in series, the total length of the sensor head will exceed 20 mm. If the bending area is shorter than this, the demodulation results may become inaccurate, and the sensitivity will be reduced. Such hybrid sensors are not suitable for measuring curvature of small structures, nor extended applications in compact sensing systems.

In this paper, we demonstrate a compact hybrid fiber sensor. The sensor head consists of an abrupt biconical taper formed using a conventional fusion splicer. The Bragg grating is inscribed into the biconical taper using an infrared femtosecond laser with phase mask. The length of the sensor is less than 0.8 mm. The FBG interacts with the abrupt biconical taper to couple the radiation from the cladding to the backward-propagating core mode, which realizes an interferometer in reflection-mode. Bending of the sensor head would reduce the coupling efficiency, which results in a change in the contrast of the interference fringes. Compared with a hybrid sensor utilizing a TFBG or LPG, our system is easier to fabricate, and is a simpler structure that is more compact; this makes it suitable for applications such as a compact fiber accelerometer or compact displacement sensor. A configuration to measure curvature utilizing bending sensors with different diameters is used to demonstrate the sensing characteristics. The temperature cross-sensitivity is studied, and we show that our system is insensitive to temperature.

2. Sensor fabrication and operating principle

The abrupt biconical taper was fabricated using a Furukawa S178 fusion splicer. The fusion splicer does not provide a taper function; however, biconical tapers with waist diameters in the range 50–125 μm can be formed from standard telecom single-mode fibers by modifying the arc time duration and increasing the fiber pulling distance. The mechanical strength of the fabricated taper will be weaker if the waist diameter is further decreased. The fabricated taper was less than 1-mm-long. Figure 1 shows an optical microscope image of a fabricated taper, which had a waist diameter of 57 μm. The length of the taper was 0.8 mm. We measured the reflection and transmission spectrum of the fabricated taper, and no interference fringes were observed. An FBG was inscribed in the taper using an amplified Ti:sapphire femtosecond laser with a center wavelength of 800 nm and a phase mask with a period of 2.14 μm. The length of the fabricated FBG was 4 mm. A femtosecond laser is a powerful and flexible tool

#234537 - $15.00 USD Received 13 Feb 2015; revised 5 Apr 2015; accepted 6 Apr 2015; published 20 Apr 2015

for microfabrication [12,13], and can be used to achieve a large refractive index modulation in various materials without required special photosensitization techniques, due to the large peak intensities and the strong nonlinear interaction between light and the materials [14,15]. The pulse duration of the laser was 150 fs, and the repetition rate was 1 kHz. The laser was focused using a 25-mm focal length cylindrical lens. A translation stage was used to scan the focused beam across the fiber with a scanning range of ± 10 μm. Gratings with a period of 1.07 μm were induced in the core and extended to the cladding of the tapered region, as shown in Fig. 1. The reflection spectrum was monitored during the write process.

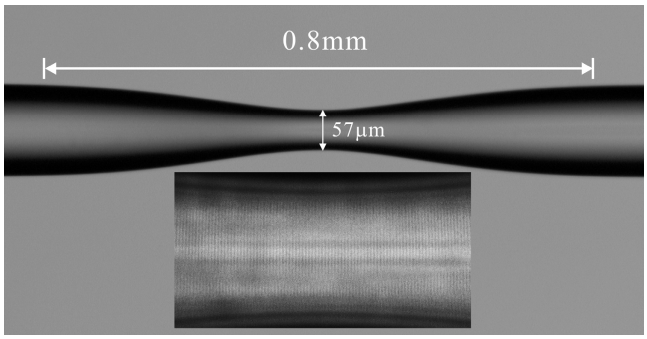

Fig. 1. Microscope image of the abrupt taper with a waist diameter of 57 μm over a length of 0.8 mm. The inset shows the grating fringes in the taper. The plane of the image is normal to the axis of the femtosecond laser beam.

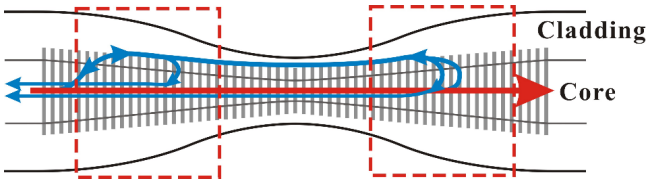

Fig. 2. Schematic diagram of the sensor. The FBG incorporating the abrupt biconical taper couples light from the cladding to the backward-propagating core mode in the taper.

Figure 2 shows a schematic diagram of the optical fiber sensor. The operating principle is as follows. For an abrupt (non-adiabatic) taper with a large taper angle, the core mode will be partially coupled into the cladding [16,17]. The mechanism of optical coupling in fiber tapers has been extensively studied by J. D. Love *et al* [18,19]. The FBG in the abrupt biconical taper couples light from the cladding to the backward-propagating core mode in the upstream and downstream taper, forming an interferometric cavity, which results in interference fringes. The light will also be coupled into the backward-propagating cladding mode from the core by the FBG at the downstream taper and re-coupled into the core at the upstream taper. The black curve in Fig. 3(a) shows a reflection spectrum of the fabricated sensor with a taper waist diameter of 57 μm. The reflection peak on the long-wavelength side results from the Bragg resonance, where the central wavelength was 1550 nm. On the short-wavelength side of the Bragg resonance, we can see interference fringes with a maximum contrast of approximately 12.5 dB and a wavelength range from 1525 nm to 1548 nm. The period of these interference fringes is $\Delta\lambda = \lambda^2/2n_{eff}L_{eff}$ where λ is the wavelength, n_{eff} is the effective refractive index of the fiber and L_{eff} is the effective length of the interferometric cavity. For the optical fiber, we have n_{eff} = 1.465. For the sensor shown in Fig. 3(a), the period of the interference fringes at 1535.6 nm was approximately 1.3 nm, corresponding to L_{eff} = 619.1 μm, which is similar to the length of the biconical taper (0.8 mm). This result is in good agreement with our inferred operating principle. An FBG inscribed in non-tapered fiber was also fabricated and the transmission spectrum was measured, in which no transmission dips were observed at the spectral range where interference fringes present. The result suggests

#234537 - $15.00 USD Received 13 Feb 2015; revised 5 Apr 2015; accepted 6 Apr 2015; published 20 Apr 2015

that the FBG expanding to the outside of the tapered region do not play a part in the interference.

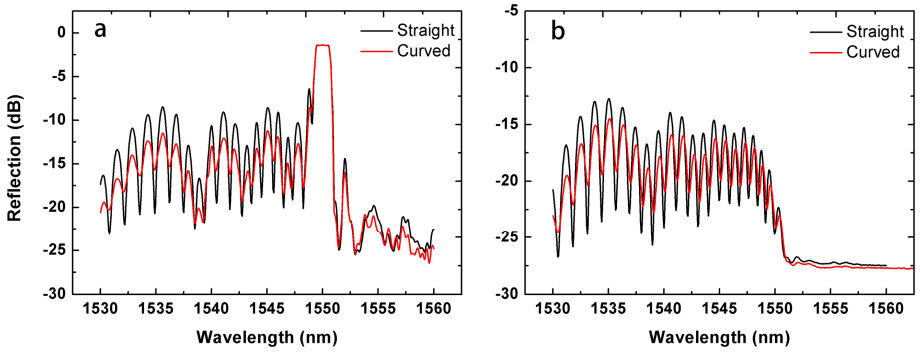

Fig. 3. Reflection spectra for straight and curved fibers. (a) The sensor with a 4-mm-long FBG and (b) the sensor with a short FBG inscribed only in the tapered region.

Bending deformation of the biconical taper will lead to changes in the coupling efficiency and transmission loss, and the amount of energy that is coupled back into the backward-propagating core mode; this will result in a decrease in the contrast of the interference fringes. The red curve in Fig. 3(a) shows how the spectrum changes when the sensor head is deformed. The contrast of the interference fringes decreased, and there were no significant changes in the Bragg resonance. The transmission spectrum of the sensor was also measured. However, the transmission dips related to the interference have a depth of only 0.3 dB, which are not as usable as the fringes in reflection-mode.

Using the default settings, the fabricated FBG will be approximately 4-mm-long. The taper is in the center of the FBG. By reducing the length of the exposed area, we also fabricated a sensor head with a very short FBG inscribed only in the tapered region. The length of the FBG is about 1 mm. The black curve in Fig. 3(b) shows the reflection spectrum of the sensor, which had a waist diameter of 65 μm. There is no Bragg resonance as seen in Fig. 3(a), which indicates that there are no gratings outside the tapered region. The red curve shows the contrast of the interference fringes decrease when the sensor is deformed, which is consistent with the data shown in Fig. 3(a). These results suggest that the functional area related to the interference fringes is in the tapered region, and the FBG extending to the outside of the tapered region does not influence the interference fringes.

3. Experiment and discussion

To investigate the orientation dependence, a sensor head was deformed with a curvature of about 80 m^{-1}. The bending direction was rotated relative to the incidence direction of the fabrication laser beam. The changes in the contrast of the fringes at the leftmost peak of spectrum envelope were measured, which is shown in Fig. 4. The maximum and minimum contrast change of −8.31 dB and −4.12 dB was achieved at 180° and 0°, respectively. There are two factors leading to the orientation dependence. One is that the distribution of the index modulation of the FBG inscribed in the taper is asymmetry and the other is the angular dependence of the coupling efficiency at the tapered region. As a consequence, the bending sensor shows orientation sensitivity.

To demonstrate the sensing characteristics of the FBG bending sensor, we used a curvature measurement configuration, as shown in Fig. 5(a). Three fabricated sensors were used, which had waist diameters of 57 μm, 65 μm, and 78 μm. The sensor with a waist diameter of 65 μm was fabricated with the FBG inscribed only in the tapered region. The sensor was fixed on a thin plastic beam, which was fixed on a block at one end, and the other end was displaced using a translation stage. To avoid strain along the fiber, only one end of the sensor was fixed. The contact point was 5 mm from the fixed point, and the sensor head was located midway between these two end-points. The plastic cantilever beam was displaced

#234537 - $15.00 USD Received 13 Feb 2015; revised 5 Apr 2015; accepted 6 Apr 2015; published 20 Apr 2015

in steps of 0.2 mm, up to a maximum of 1.4 mm. The bending direction was set to 180°, where the sensor would show the highest sensitivity. The reflection spectra were recorded, and the decrease in the contrast of the fringes at the leftmost peak of spectrum envelope was measured as an indicator of the curvature. The curvature at the center of the cantilever is $1/R \approx 3d/2l^2$, where d is the displacement and l is the length of the cantilever beam.

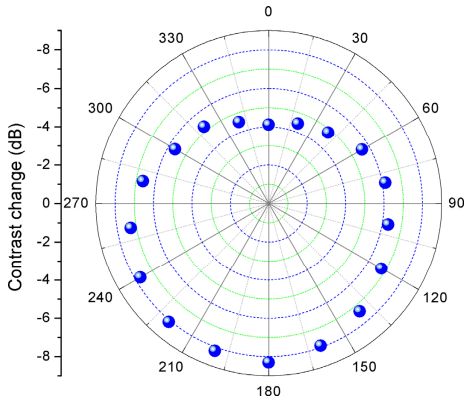

Fig. 4. Orientation dependence of the sensor head.

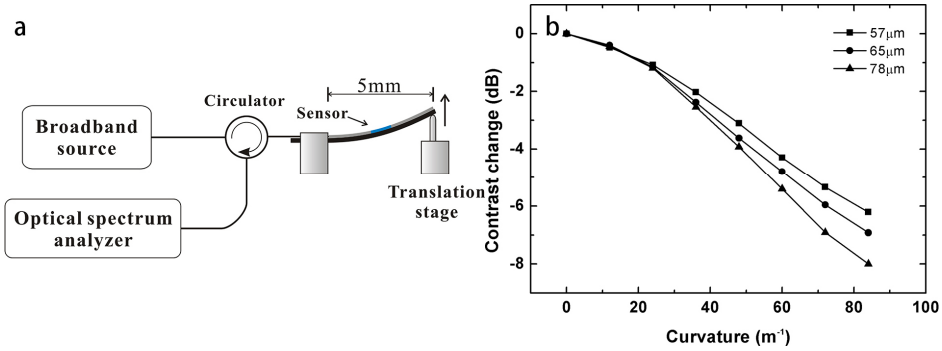

Fig. 5. (a) Configuration used for the curvature measurements. (b) Changes in the contrast of the interference fringes as a function of the curvature.

The changes in the contrast of the interference fringes as a function of the curvature are shown in Fig. 5(b) for the three sensors with different waist diameters. The measured sensitivity was 0.1196 dB/m^{-1}, 0.1004 dB/m^{-1}, and 0.0946 dB/m^{-1}, for the 57 μm, 65 μm, and 78 μm diameter sensors, respectively. The sensitivity is not as high as the sensors combing TFBGs with other structures. However the sensors based on TFBGs or LPGs with a high sensitivity are usually achieved in a device length of over 20 mm. The sensitivity increased as the waist diameter decreased. Because the mechanical strength of cantilever is much higher than the fiber, the curvature is mainly related to the cantilever. The increase of the sensitivity mainly results from that the coupling efficiency and transmission loss of the hybrid structure with the thinner waist will change more when the fiber is deformed. The spectral response of the sensor with a short FBG inscribed only in the tapered region was in good agreement with the other two. This result is consistent with the operating principle of the sensor being independent of the grating away from the tapered region.

To investigate the temperature response, we fabricated a sensor with a waist diameter of 55 μm, and fixed it in a breaker filled with water. A thermocouple was placed near the sensor head in the water, and the temperature was varied in the range 20–70°C. The changes in the contrast of the interference fringes were minimal, as shown in Fig. 6(a). The wavelength shift was linear with a temperature sensitivity of approximately 0.01 nm/°C. The change in

#234537 - $15.00 USD Received 13 Feb 2015; revised 5 Apr 2015; accepted 6 Apr 2015; published 20 Apr 2015

contrast as a function of temperature was calculated using the fringe at the leftmost peak of spectrum envelope, which was the same as in the curvature measurement. The results are shown in Fig. 6(b). The fluctuation in contrast was less than 0.06 dB. Because of this small temperature cross-sensitivity, these structures have potential applications as compact curvature and temperature dual-parameter sensors. The interference fringes and the Bragg peak shift by about the same amount with temperature increased, which is a normal phenomenon. The temperature sensitivity of the interference fringes is $\kappa_f = \alpha\lambda_f/n_{eff}$, where α is the thermo-optic coefficient and λ_f is the wavelength of the interference fringe. The temperature sensitivity of the Bragg resonance is $\kappa_{Bragg} = 2\alpha\Lambda_G/m$, where Λ_G is the grating period and m is the order of the FBG. Then we can get κ_f: $\kappa_{Bragg} = \lambda_f/\lambda_{Bragg}$. The second order Bragg wavelength λ_{Bragg} is 1550nm. For λ_f of 1535 nm, then κ_f: κ_{Bragg} = 0.99. So when the temperature is increased, the interference fringes and the Bragg peak shift at about the same rate. By monitoring the contrast and the wavelength shift of the interference fringes, the curvature and temperature can be measured simultaneously.

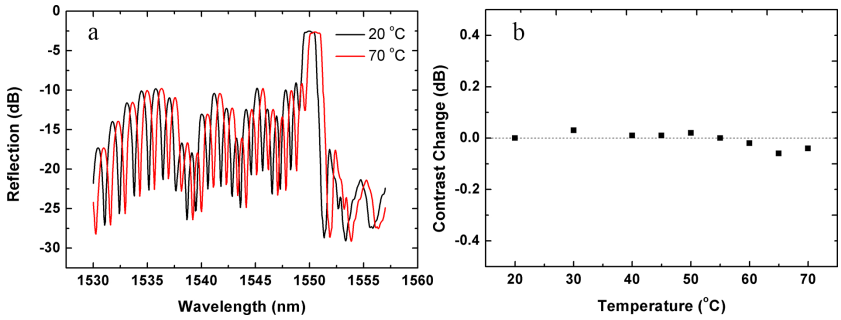

Fig. 6. (a) Reflection spectra of the sensor at temperatures of 20°C and 70°C. (b) Change in the contrast of the interference fringes as a function of temperature.

4. Conclusion

We have demonstrated a compact bending sensor based on an optical fiber with an FBG and an abrupt biconical taper. The sensor head consisted of a biconical fiber taper formed using a conventional fusion splicer, in which an FBG is inscribed using a femtosecond laser. This optical fiber sensor is advantageous compared to the conventional hybrid fiber bending sensors because of the facile fabrication, simple structure, and compact size, which make it suitable for the measurements of the curvature and displacement of small structures and extended applications of compact sensing systems. We have demonstrated a configuration to measure curvature using this optical fiber sensor. Furthermore, we have shown that the sensor has low temperature cross-sensitivity, which makes it suitable for applications as a compact curvature and temperature dual-parameter sensor.

Acknowledgments

The authors gratefully acknowledge the financial support for this work provided by the National Basic Research Program of China (973 Program) under Grant No. 2012CB921804, and the National Natural Science Foundation of China (NSFC) under the Grant Nos. 61235003, 11204236, and 61308006. This work was also supported by collaborative innovation center of Suzhou nano science and technology.